

Chapter 8: Synthesis of Asymmetric Spectral Lines

8.1: Adapting the Plane-Parallel Approximation

With the parametric granular cell model (as discussed in chapter 7), the emergent spectrum can be found by using plane-parallel spectral synthesis methods. Although the granulation results in the plane-parallel approximation breaking down in a global sense, it can still be used locally, in regions which are approximately plane-parallel.

It is desirable to have as few regions as necessary, both to reduce computational requirements, and to keep the number of free parameters in the granulation model as low as possible.

The basic procedure is then quite simple for the upflow and downflow regions which are plane-parallel regions with vertical velocity gradients (and possibly microturbulence gradients). The only region presenting any difficulty is the transition region between the upflow and downflow regions.

8.1.1: The Granule-Intergranular Space Transition Region

Difficulties arise in the treatment of the transition region as there is a horizontal variation in the vertical velocities in this region. This, coupled with the vertical gradient of the vertical velocities, results in a plane-parallel treatment, strictly speaking, being incorrect. The plane-parallel calculation is desirable, so the importance of deviation from plane-parallelism should be determined.

The deviation from plane-parallelism is the variation of the vertical gradient of the vertical velocity with horizontal position (see figure 8-1).

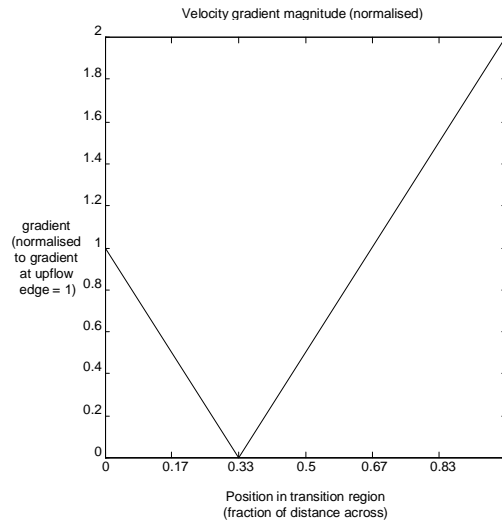


Figure 8-1: Horizontal Variation of Vertical Velocity Gradient

The vertical velocity gradient is proportional to the vertical velocity, so the variation of the gradient across the transition region is proportional to the variation of the magnitude of the vertical velocity (see figure 6-2).

Where there is no vertical velocity gradient (where the vertical velocity is zero), the vertical velocity gradient will have no effect on the spectrum emergent from this portion of the transition region. Where the vertical velocity gradients are greatest (at the edges of the region), the spectrum will be affected by the height-dependent Doppler shift of the line absorption profile.

There are two simple techniques that can be used. Firstly, line broadening due to the vertical velocity variations within the region can be treated as non-Gaussian microturbulence. The opacity at a particular depth can be convoluted with the distribution of Doppler shifts due to the flow velocities. Secondly, the emergent spectrum can be found, and then broadened by the Doppler shift distribution.

The first of these techniques is preferable, as the second cannot adequately take the height dependence of the flow velocity into account. The second, however, can be used in order to estimate errors introduced by the first method being used.

A similar problem arises when considering the variation between granules, represented in the parametric model by the macroturbulence. As the macroturbulence affects the velocity gradients, rather than simply broadening the lines, treating it identically to traditional macroturbulence is an approximate method only. Errors

introduced by this approximation will be greater for strong lines than for weak lines, which are less dependent on broadening processes.

8.2: The Granular Cell Model

The parametric granular cell model was developed in chapter 7, using observational data on granulation whenever possible. The granular cell is represented by sixteen parameters, not all of which can be freely chosen. The model has eleven free parameters, some of which are reasonably well determined by observations.

8.2.1: The Granular Cell Model

The model consists of three regions: the upflowing granular centre, the downflowing intergranular space, and the transition region between them, denoted respectively by the subscripts U , D , and T . There are five parameters describing each region, and one global parameter. The five local parameters are the area, the brightness, the flow velocity, the microturbulent velocity, and the macroturbulent velocity.

The area parameters A_u , A_d , and A_t are the fractions of the surface occupied by the regions. The brightness parameters B_u , B_d , and B_t are used to weight the contributions from the different regions to account for the differing continuum intensities emergent from these regions. The effect of the brightness parameter depends on the wavelength (see equation (7-8)), so the contribution of a region to the spectrum is proportional to

$$I_{adjusted} = A_i \left(1 + \frac{5000}{\lambda} (B_{5000} - 1) \right) I_{\lambda i}. \quad (8-1)$$

The other parameters affect the formation of the spectrum within the region. The global parameter is the velocity scale height V_s , with which the flow velocities (and the microturbulent velocities if depth dependence is assumed) are assumed to vary exponentially. The flow velocity for an upflow region i at a height h is

$$V_U = V_0 e^{-\frac{h}{V_s}} \quad (8-2)$$

and the upflow and downflow velocities are related by the area parameters using equations (7-10) and (7-12). The flow velocity in the transition region will vary from the upflow velocity to the downflow velocity. If depth-dependent microturbulence is being used, the microturbulent velocity is

$$\xi_i = \xi_{0i} e^{-\frac{h}{V_s}}. \quad (8-3)$$

The macroturbulence parameters ΔV_U , ΔV_T , and ΔV_D account for the variation between granules, and are used in the same manner as macroturbulence in the traditional macroturbulence-microturbulence convection model.

8.2.2: The Model Parameters

The initial values adopted for the granular model parameters are shown in table 8-1.

Table 8-1: Initial Granular Model Parameters

Parameter	Upflow U	Transition T	Downflow D	All
A	0.45	0.4	0.15	–
B	1.07	0.97	0.87	–
V_0	–	–	–	0.577 kms ⁻¹
V_s	–	–	–	368 km
depth dependent ξ	0.95 kms ⁻¹	4.27 kms ⁻¹	4.27 kms ⁻¹	–
depth independent ξ	0.3 kms ⁻¹	1.35 kms ⁻¹	1.35 kms ⁻¹	–
ΔV	0.25 kms ⁻¹	0.3 kms ⁻¹	0.5 kms ⁻¹	–

The initial parameter values have been determined from observations of the solar granulation. There are large uncertainties in a number of them, particularly the microturbulence and the macroturbulence parameters. The closeness of the fit between

the observed and computed line profiles can be used to adjust the values of the parameters. This is done by adjusting the desired parameters until the squared deviation between the observed and computed data points

$$\Delta = \sum (I_{obs} - I_{calc})^2 \quad (8-4)$$

is a minimum.

It is expected that this will prove necessary for the macroturbulence parameters. It may prove impossible to fit some of the parameters accurately, as a number of the effects of different parameters may prove difficult to separate. For example, both the area and brightness parameters have similar effects, and distinguishing between microturbulence and macroturbulence is difficult unless accurate damping constants and oscillator strengths are available.

8.2.3: Comparison with other Convective Cell Models

Purely plane-parallel convective cell models, despite their limitations, have been used in the past. Such models typically use a high velocity gradient when reproducing the asymmetry present in solar lines. The value of such models is examined in section 8.3.3 where the effect of the velocity gradient on asymmetry is investigated.

Multi-stream models (of which the model used here is an example) have also been used. Simple multi-stream models which do not properly account for the structure of the granulation fail to reproduce observed spectra. A multi-stream model with a sufficient number of columns and free parameters will, given appropriate parameter values, be able to reproduce the observed spectrum.¹ If such a model has an excessive number of free parameters, the values obtained by such a fit are unreliable. For this reason, care has been taken here to have as few free parameters as possible in the adopted granular model.

¹For an example of such a model (a four-column model similar to the model used here, but with less detailed modelling of flow velocities and microturbulence), see Dravins, D. "Stellar Granulation VI: Four-Component Models and Non-Solar-Type Stars" *Astronomy and Astrophysics* **228**, pg 218-230 (1990). As stellar granulation cannot be directly observed, it is necessary in such cases to obtain all parameter values by fitting observed and calculated spectra.

Granular motions directly calculated, such as the numerical granular simulations by Nordlund and others, can also be used to calculate spectra. As the behaviour of such simulated granulation is time-dependent, the calculated spectrum must be averaged over enough spatial points and time points so as to produce a reliable average spectrum. This procedure is demanding on computational capacity.

8.3: Spectral Synthesis with the Convective Cell Model

8.3.1: Comparison between Predicted and Observed Spectra

The granular model was used to calculate emergent spectra for a number of spectral lines. The initial parameters were adjusted as required to produce the best agreement between the observed and computed spectra. The depth-dependent microturbulence model was found to give a better fit to the observed spectrum than the depth-independent model. Accordingly, the depth-independent model was discarded.

Examples of the agreement between the observed and calculated spectra are shown in figures 8-2, 8-3, 8-4, 8-5 and 8-6. (Plane-parallel fits for the same lines are shown in figure 5-9, 5-10, 5-11, 5-12 and 5-13.)

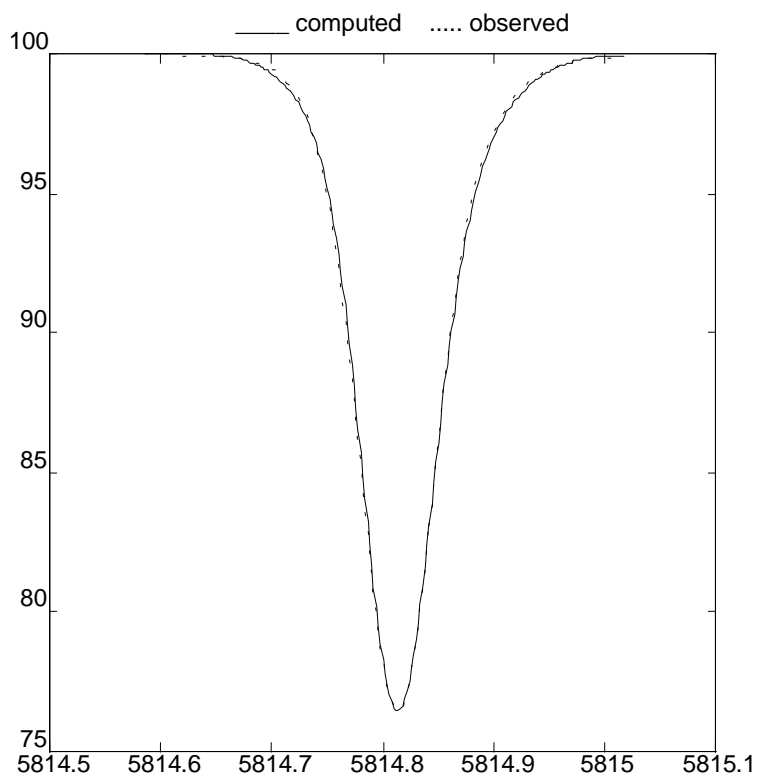


Figure 8-2: Fe I at 5814.814 Å

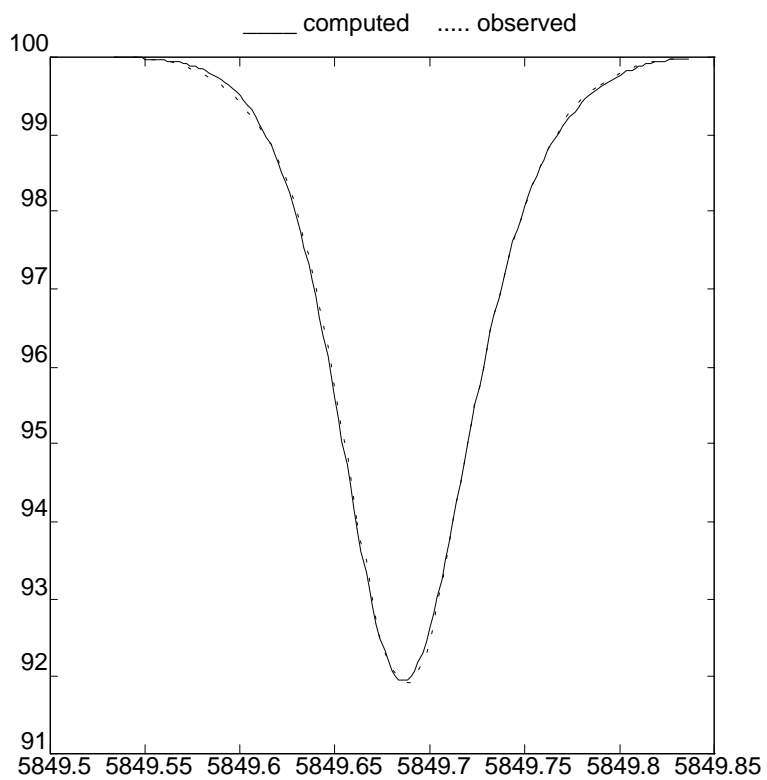


Figure 8-3: Fe I at 5849.687 Å

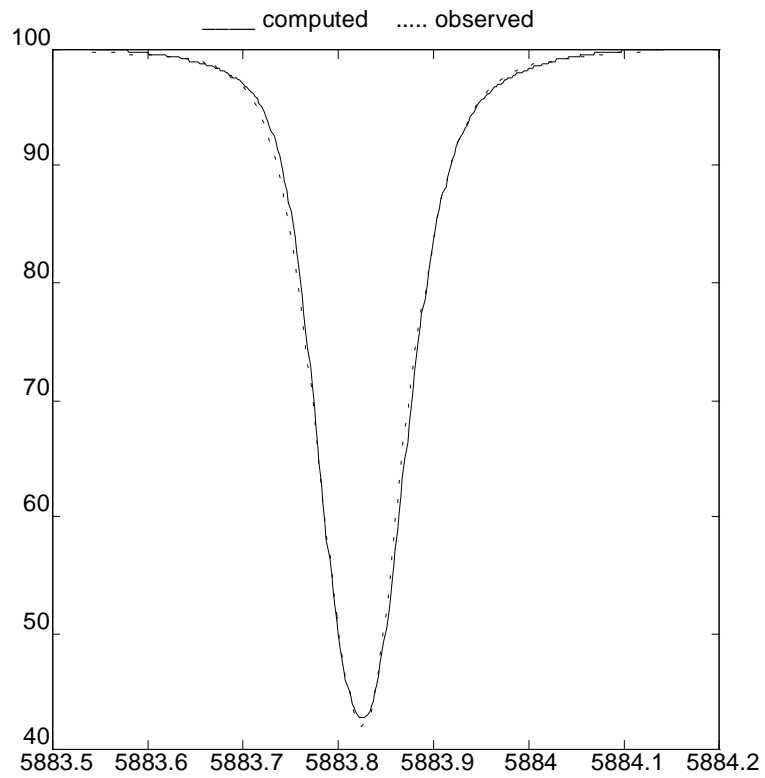


Figure 8-4: Fe I at 5883.823 Å

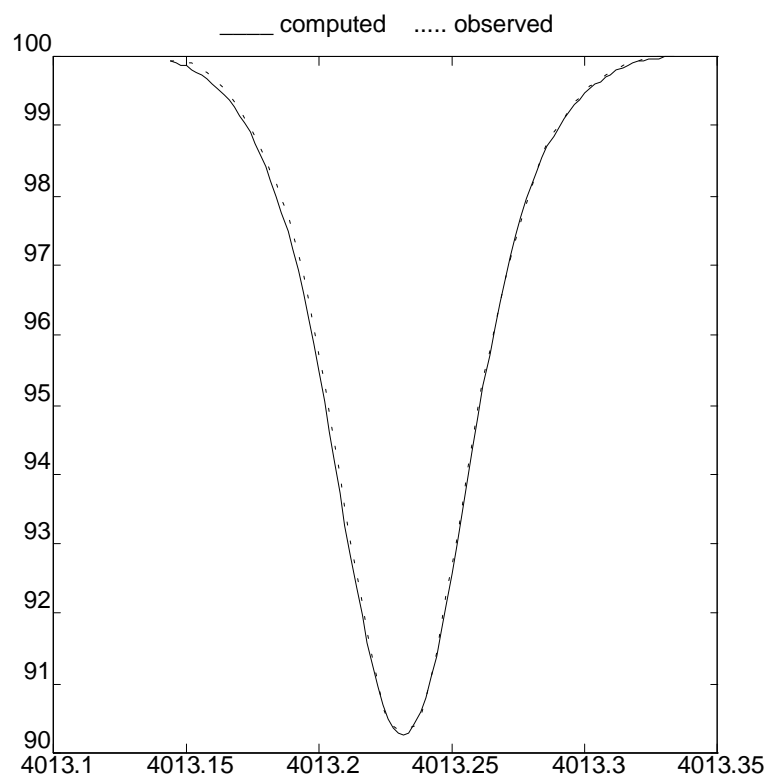


Figure 8-5: Ti I at 4013.232 Å

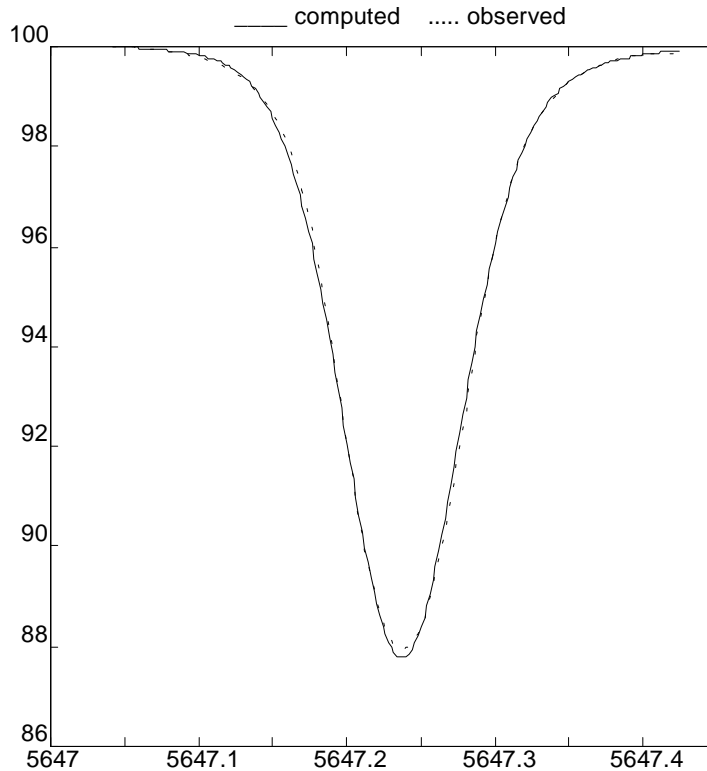


Figure 8-6: Co I at 5647.238Å

The spectra calculated using the granular model fit the observed spectra more closely than the best fits obtainable using the purely plane-parallel microturbulence-macroturbulence model (see section 8.3.5 for a quantitative analysis of the improvement). The asymmetry in the observed spectral lines is reproduced by the calculated line profiles.

The closeness of the fit between the observed and computed spectra shows clearly that the granular motions are responsible for the asymmetry of solar lines.

Other lines can be readily calculated with similar accuracy. The difference between the observed and computed spectra is examined in 8.3.4.

8.3.2: Final Parameter Values

The final parameter values for the model (with depth-dependent microturbulence) are shown in table 8-2.

Table 8-2: Final Parameter Values

Parameter	Upflow U	Transition T	Downflow D	All
A	0.45	0.4	0.15	–
B	1.07	0.97	0.87	–
V_0	–	–	–	0.577 kms^{-1}
V_s	–	–	–	368 km
ξ	1.58 kms^{-1}	3.67 kms^{-1}	3.67 kms^{-1}	–
ΔV	$1.6 \pm 0.2 \text{ kms}^{-1}$	$1.6 \pm 0.3 \text{ kms}^{-1}$	$3.5 \pm 1.1 \text{ kms}^{-1}$	–

The parameters modified were the microturbulence and macroturbulence parameters. Substantial increases were made to the macroturbulence parameters. The other parameters were not modified as the initial estimates of their values were more reliable, and it was not necessary to modify them in order to produce a close fit between the observed and computed spectra. The errors in these parameter values are discussed in section 8.3.4.

8.3.3: The Effect on the Spectrum

The contributions to the spectrum from each of the regions are shown in figure 8-7. The contributions shown are not adjusted for the area and brightness of the region.

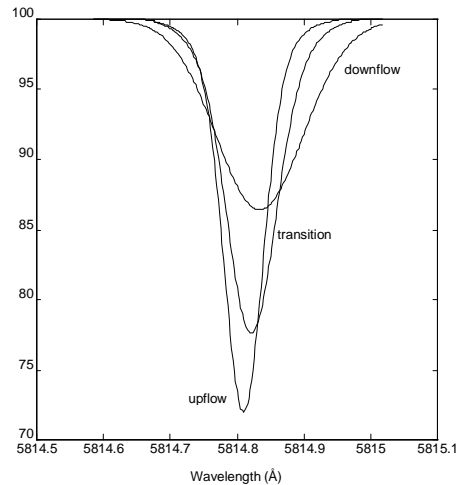


Figure 8-7: Contributions from Regions for Fe I at 5814.814Å

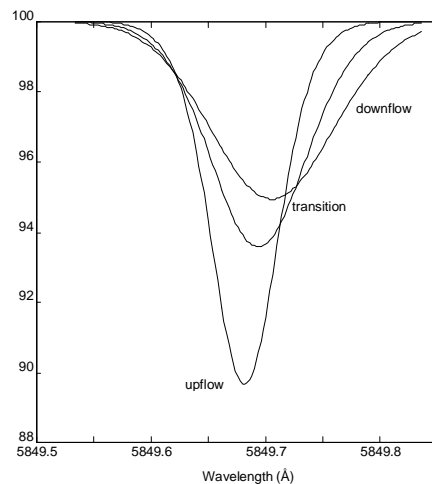


Figure 8-8: Contributions from Regions for Fe I at 5849.687Å

The asymmetry in the resultant profile is predominantly due to the red- and blue-shifts of the components. The velocity gradient, which affects each of the individual components, has only a small effect on the overall spectrum. The contributions from the individual regions, as expected, resemble observed high spatial resolution spectra.² Both the upflow and downflow region spectra show the asymmetry observed in spectra emergent from upflows and downflows.

²See Kiselman, D. "High-Spatial-Resolution Solar Observations of Spectral Lines Used for Abundance Analysis" *Astronomy and Astrophysics Supplement Series* **104**, pg 23-77 (1994) and Hanslmeier, A., Mattig, W. and Nesis, A. "High Spatial Resolution Observations of Some Solar

The asymmetry due to the velocity gradient (such as the asymmetry observed in the upflow contribution) cannot account for the asymmetry observed in the spatially averaged line profile. The asymmetry in the upflow due to the velocity gradient is, as expected, the opposite of the asymmetry in the mean spectrum. Therefore, any model of granulation using only the velocity gradient to produce the observed asymmetry is inherently unphysical, and will not yield useful information on granular velocities.

The importance of the upflow region is readily seen from the individual contributions. Weighting the contributions by the area and brightness parameters will increase the upflow contribution and decrease the downflow contribution.

8.3.4: Errors in Parameters

The values for the macroturbulence and microturbulence parameters are difficult to separate, as they have similar effects on the spectrum. The line strength is affected by the microturbulence, and not by the macroturbulence, so if accurate oscillator strengths and damping constants are known for a number of lines, they can be individually determined. The gf -values available for the lines examined here are not sufficiently accurate for such a determination to be reliable.

The approximations inherent in the model must also be considered. The three major approximations in the model adopted here are the simplistic treatments of the temperature variation between regions and the variation between individual granules, and the modelling of the transition region. The first of these, where the temperature variations are represented in terms of a brightness parameter, can be removed if separate model atmospheres are constructed for each region with different temperature profiles. As the simple model produces good synthetic spectra, such an undertaking is not overly useful.

Photospheric Line Profiles” *Astronomy and Astrophysics* **238**, pg 354-362 (1990). As the calculated contributions represent the average spectra emergent from all upflows, all downflows, and all transition regions, the calculated spectra should be broader than observed spectra from single small elements. However, if the observed areas are larger than single flow regions, the observed spectra will be broader. However, a qualitative comparison readily shows the similarity.

The simple treatment of intergranular variation of velocities as Gaussian macroturbulence would require accurate measurement of velocities of different regions. While velocity measurements of this nature have been carried out,³ they fail to separate measurements of granular centres and intergranular regions. With velocity measurements of different regions not separated, it is difficult to determine the range of velocities present for a particular region.

The modelling of the transition region can be improved by dividing it into a number of smaller regions. This is considered in more detail in section 8.4.1.

The closeness of the fit between the observed and computed spectra can be investigated. The difference between separate observations of the line profiles can be used as an estimate of the accuracy of the observed profiles. Figure 8-9 and 8-10 compare the difference between the computed and observed spectra with the difference between two sets of observed spectra.

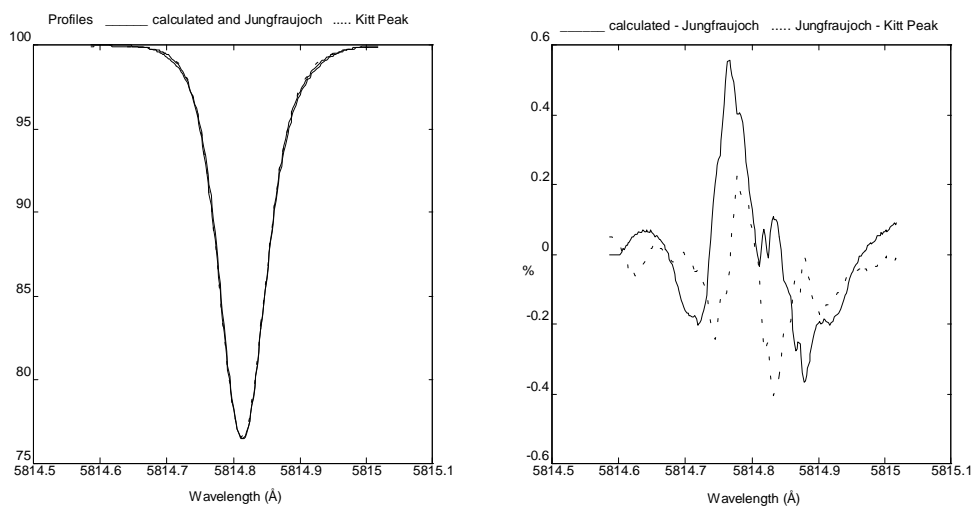


Figure 8-9: Error in Fit for Fe I at 5814.814Å

³Bumba, V. and Klvana, M. "Doppler Velocity Measurements Made with a Scanning Photoelectric Magnetograph" *Solar Physics* **160**, pg 245-275 (1995).

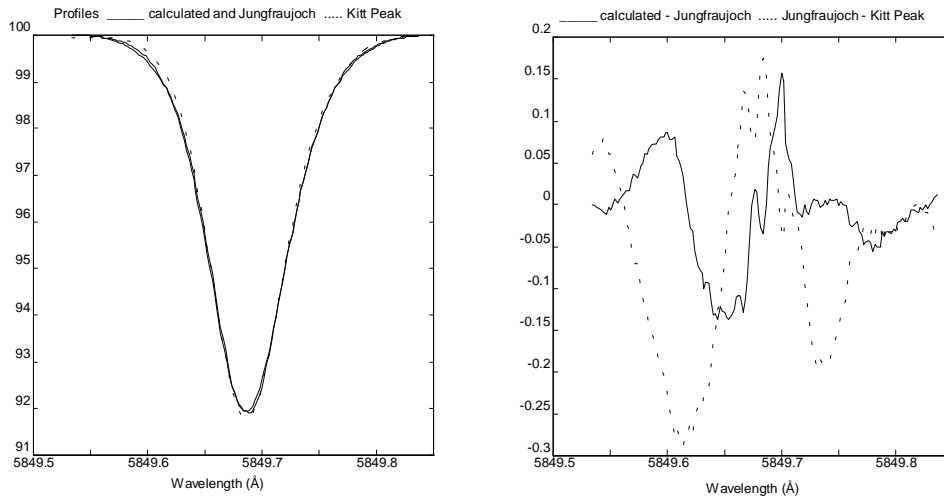


Figure 8-10: Error in Fit for Fe I at 5849.687Å

The calculated spectra match the observed spectra to approximately the accuracy of the observed data. Thus, there is little gain in attempting to further improve the fit between calculated and observed spectra. The parameter values used can therefore be used with a reasonable degree of confidence. If necessary, the microturbulence and macroturbulence parameters can be adjusted for individual lines, but the other parameters should require little change, if any.

8.3.5: Goodness of Fit of Lines Compared with Standard Model Fits

The accuracy of the best fits obtainable between calculated and observed spectra for the lines studied can be measured quantitatively. A suitable measure of goodness of fit is the total squared deviation (defined by equation (8-4)). The maximum value of the squared deviation measured at a single wavelength point is of interest. Using abundance values giving the best fit for each line⁴, the resulting deviations are shown in figures 8-11 and 8-12.

⁴Neglecting the potassium line at 7698.974Å, which is expected to require a full non-LTE treatment and is not well fitted by either model.

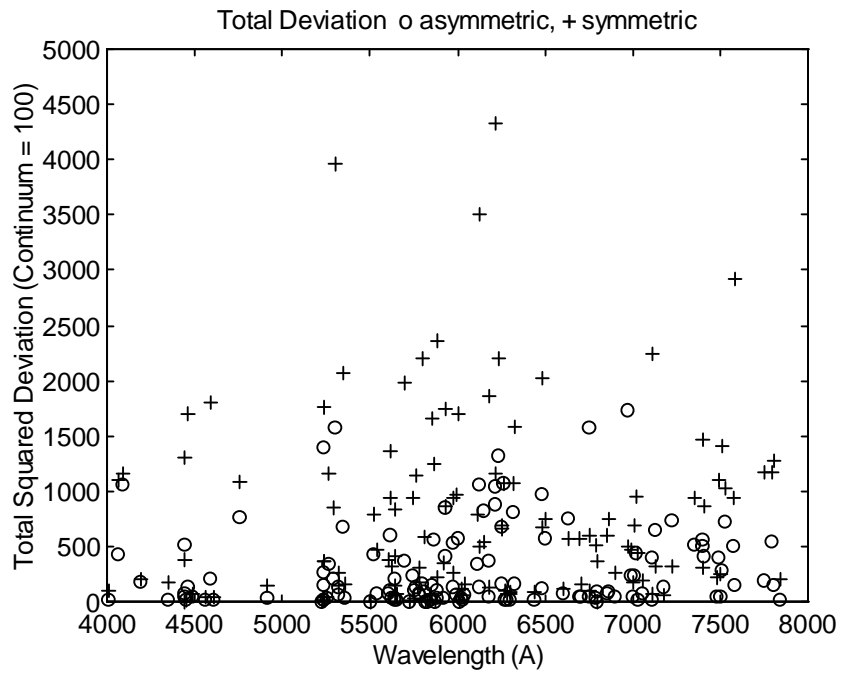


Figure 8-11: Total Squared Deviation Between Observed and Calculated Spectra

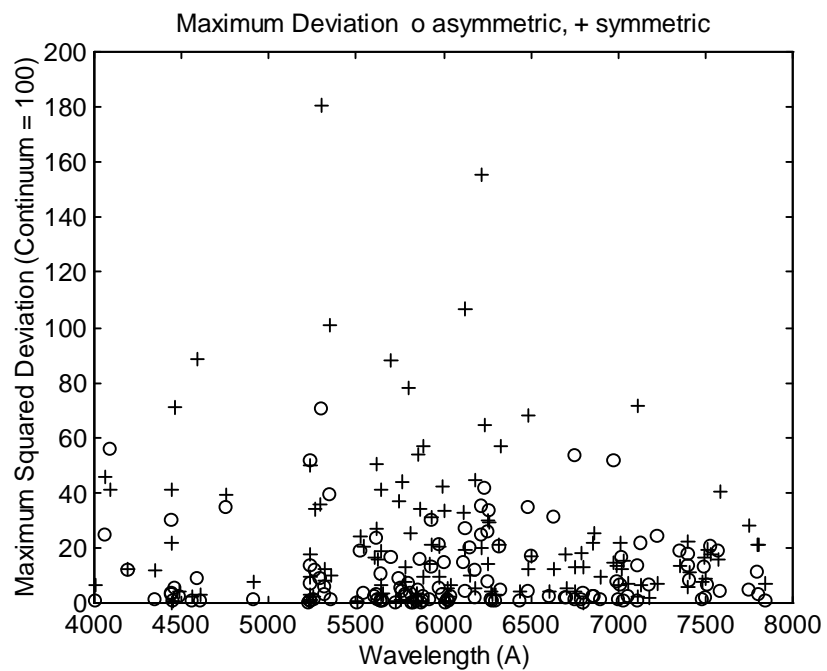


Figure 8-12: Maximum Squared Deviation Between Observed and Calculated Spectra

The improvement resulting from the use of the full convective cell model can be readily seen. Numerical results are summarised in table 8-3.

Table 8-3: Improvement in Goodness of Fit

Model	Total Squared Deviation (continuum = 100)	Maximum Squared Deviation (continuum = 100)
micro/macroturbulence	733.6	23.02
convective cell	287.0	10.38

It is also of interest to compare the deviations for the lines as a function of line strength or the excitation energy of the lower level. A comparison is shown in figures 8-13, 8-14, 8-15 and 8-16.

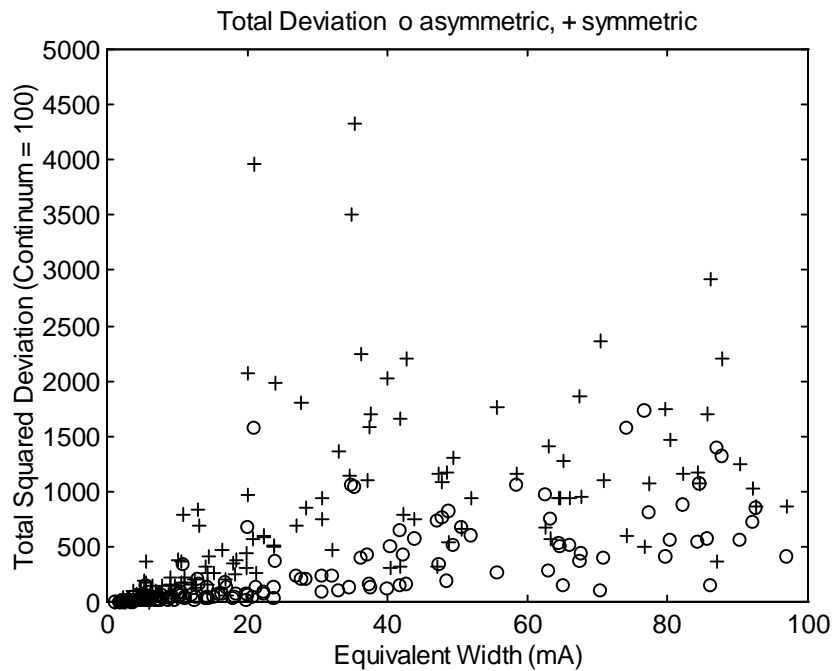


Figure 8-13: Total Squared Deviation Variation by Line Strength

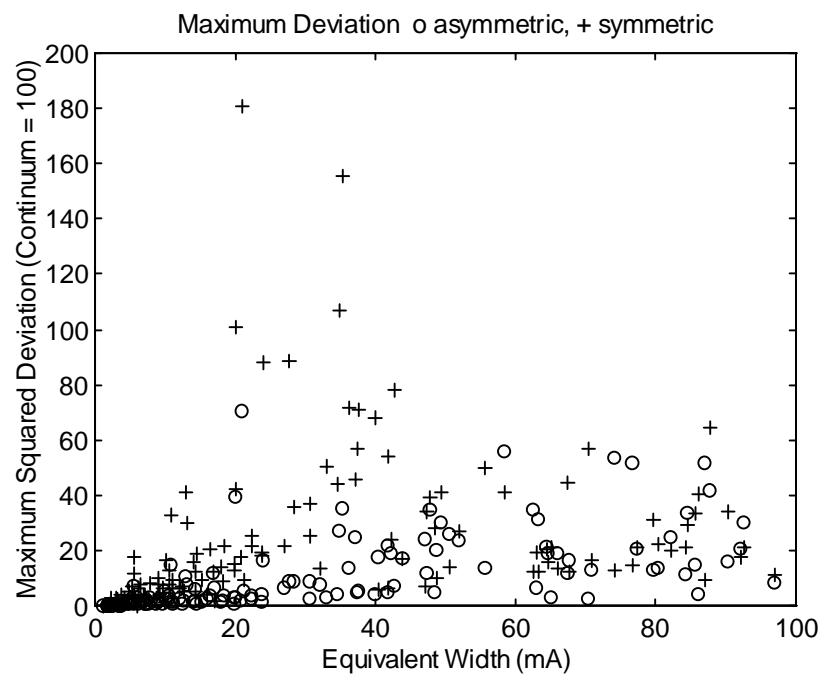


Figure 8-14: Maximum Squared Deviation Variation by Line Strength

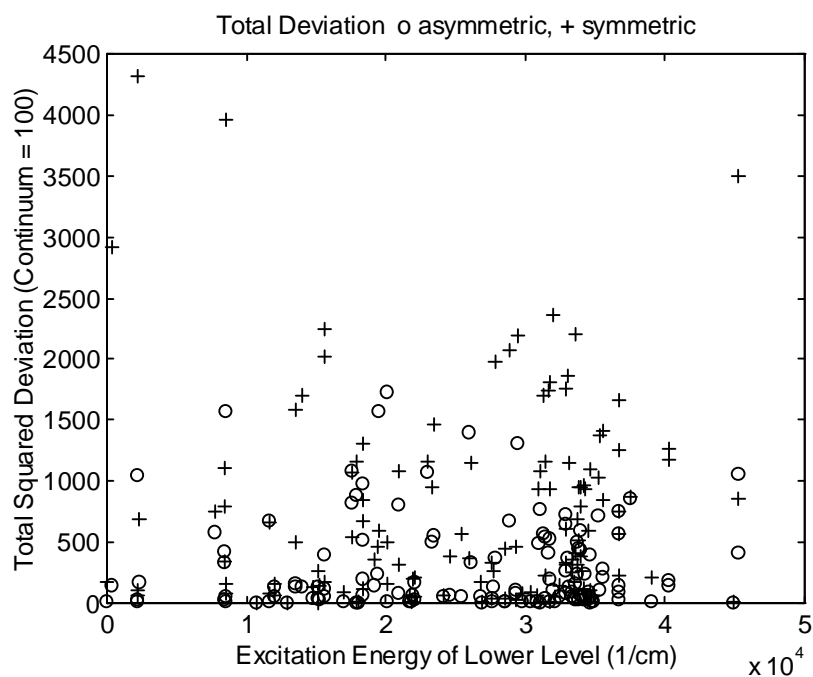


Figure 8-15: Total Squared Deviation Variation by Excitation Energy

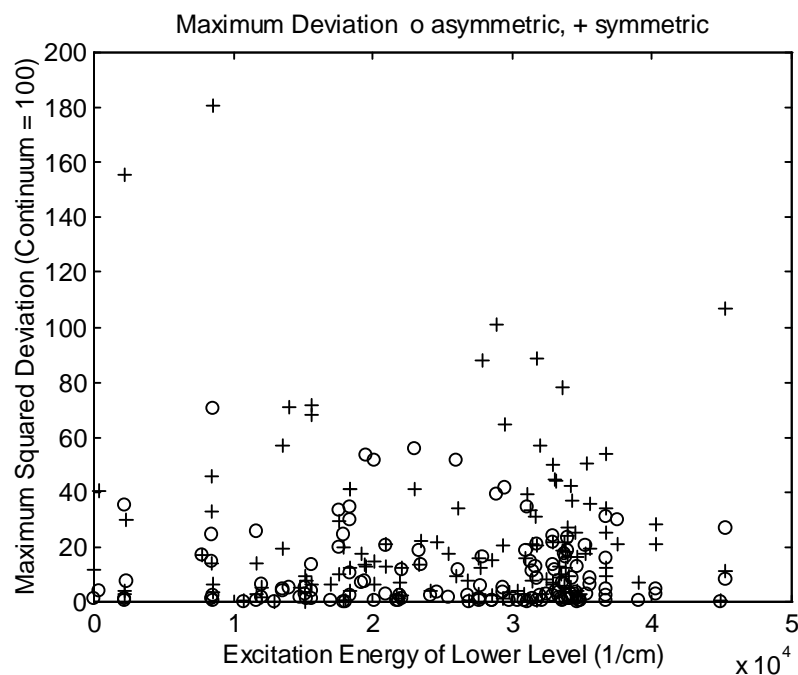


Figure 8-16: Maximum Squared Deviation Variation by Excitation Energy

The improvement in fit can be seen at all line strengths and excitation energies.

8.3.6: Asymmetric Abundance Analysis

An abundance analysis can be performed using the convective cell model to match observed and calculated spectral line profiles until the closest match is obtained. The results of such an abundance analysis are show in table 8-4.

Table 8-4: Photospheric Abundances

Element	Lines	Asymmetric Model	Standard Model	Standard Solar	Meteoric
Si	2	6.71	6.80	7.55 ± 0.05	7.55 ± 0.02
K	1	5.30	5.49	5.12 ± 0.13	5.13 ± 0.03
Ti	15	5.01 ± 0.11	5.02 ± 0.12	4.99 ± 0.02	4.93 ± 0.02
V	7	4.10 ± 0.08	4.10 ± 0.08	4.00 ± 0.02	4.02 ± 0.02
Cr	9	5.73 ± 0.11	5.77 ± 0.10	5.67 ± 0.03	5.68 ± 0.03
Mn	1	5.49	5.48	5.39 ± 0.03	5.53 ± 0.04
Fe	63	7.55 ± 0.04	7.62 ± 0.04	7.67 ± 0.03	7.51 ± 0.01
Co	5	4.78 ± 0.06	4.76 ± 0.05	4.92 ± 0.04	4.91 ± 0.03
Ni	17	6.24 ± 0.15	6.30 ± 0.14	6.25 ± 0.04	6.25 ± 0.02
Mo	1	2.01	1.94	1.92 ± 0.05	1.96 ± 0.02

The results obtained are similar, but not identical, to those obtained using the standard microturbulence-macroturbulence model. A significant difference is the lower value obtained for the abundance of iron, which is close to the meteoric abundance.

If further improvements in accuracy are desired, either more accurate f -values are required or more lines can be studied. Some of the lines do have accurately measured f -values⁵ and an abundance analysis can be performed on these lines alone. This results in a smaller number of lines being used, but with more reliable f -values. The elements for which very accurate f -values are known for the lines studied here are titanium and iron. The results are shown in table 8-5.

⁵See table C-2 in Appendix C. The most accurate f -values are those measured by the Oxford group (by Blackwell et al.) and Milford et al.

Table 8-5: Photospheric Abundances with Accurate f-values

Element	Lines	Asymmetric Model	Standard Model	Standard Solar	Meteoric
Ti	6	4.97±0.03	4.99 ± 0.02	4.99 ± 0.02	4.93 ± 0.02
Fe	12	7.46±0.05	7.55 ± 0.04	7.67 ± 0.03	7.51 ± 0.01

An improvement results from restriction of lines to the accurate f-value lines. The iron abundances using both models are now in agreement with the meteoric iron abundance. If it was possible to use a large number of lines with reliable f-values a better result could be obtained, but the number of available reliable f-values falls short of the number of useful solar lines.

8.3.7: Use of the Cell Model to Determine Line Parameters

In principle, the convective cell model can be used to determine unknown line parameters. For a line parameter to be found accurately, accurate values for the other line parameters and well known microturbulence and macroturbulence parameters are required. The accurate determination of the microturbulence and macroturbulence parameters is discussed in section 8.3.4. Accurate element abundances must also be known.

8.4: Extensions of the Model

8.4.1: Improved Modelling of the Transition Region

A simple improvement of the granular model is to divide the transition region into a number of separate regions. If the brightness, flow velocities and macroturbulence of the transition regions are found from those of the upflow and downflow regions, no new free parameters are introduced. The only cost is an increase in computational requirements. Results obtained using a multiple transition region model are shown in figure 8-17.

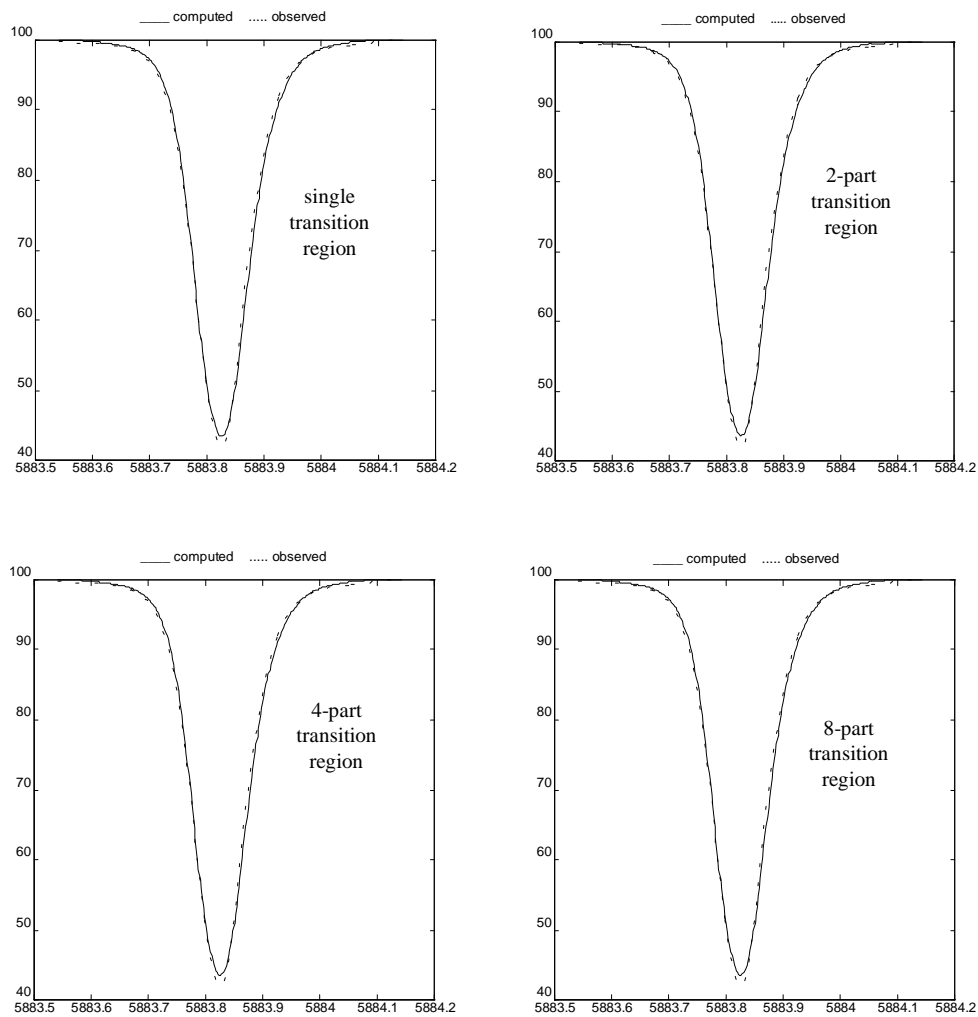


Figure 8-17: Modelling with Multiple Transition Regions - Fe I at 5883.823 Å

Improvements from the use of a multiple transition region model are most likely to be seen for strong lines. The strong Fe I line at 5883.823 Å illustrated in figure 8-17 shows very little change as the number of separate regions into which the transition region is divided is increased.

Given the close agreement between spectra calculated using the single transition region model and observed spectra, a multiple transition region model is not necessary.

8.4.2: Horizontal Motions

The three-dimensional flow velocities for a granule can be readily found. The interdependence of the horizontal flow and the gradient of the vertical flow was considered in section 6.2.3. The velocity of material flowing out from a radially symmetric region with a constant upflow can be found from equation (6-4), giving a velocity V_H dependent on the radius r of

$$V_H(r) = \frac{-r}{2} \left(\frac{dV_V}{dh} + \frac{V_V}{\rho} \frac{d\rho}{dh} \right) \quad (8-5)$$

The term in brackets can be expressed in terms of the velocity scale height V_s and the density scale height ρ_s as

$$\left(\frac{dV_V}{dh} + \frac{V_V}{\rho} \frac{d\rho}{dh} \right) = V_V \left(\frac{1}{V_s} + \frac{1}{\rho_s} \right) \quad (8-6)$$

The velocity scale height is assumed to be constant in the granular cell model, and is equal to 368 km. The density scale height in the Holweger-Muller model atmosphere is shown in figure 8-18.

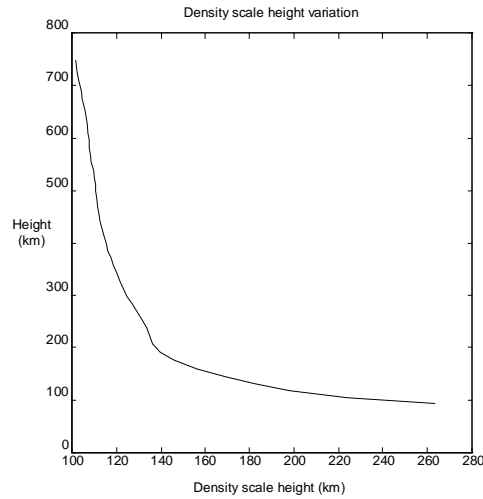


Figure 8-18: Density Scale Height in the Holweger-Muller Model Atmosphere

At greater depths, the higher degree of ionisation and the resultant increase in the electron pressure strongly affects the density. As the density scale height decreases as the height increases, this will tend to increase horizontal motions with height. The

vertical flow velocities decrease with height (in the region where spectral lines form), so this will tend to decrease horizontal motions with height.

The horizontal velocity as a function of position within a circular rising granular centre (an upflow region) with outer radius R_U is

$$V_H(r) = \frac{rV_U}{2} \left(\frac{1}{V_s} + \frac{1}{\rho_s} \right) \quad (8-7)$$

When the upflow is not at a constant velocity with respect to horizontal position (i.e. when the transition or downflow regions, or portions thereof are included), the total upflow contributing to the downflow must be found through integration.

For a circular granule of radius R , with outer radii of R_U and R_T for the upflow and transition regions respectively, the horizontal velocities in the transition region ($R_U < r < R_T$) are

$$V_H(r) = \frac{1}{2r} \left(\frac{1}{V_s} + \frac{1}{\rho_s} \right) \times \left\{ V_U r^2 + \frac{V_D - V_U}{R_T - R_U} \left(\frac{2}{3} r^3 - R_U r^2 + \frac{1}{3} R_U^3 \right) \right\} \quad (8-8)$$

and

$$V_H(r) = \frac{1}{2r} \left(\frac{1}{V_s} + \frac{1}{\rho_s} \right) \times \left\{ V_U R_T^2 + \frac{V_D - V_U}{R_T - R_U} \left(\frac{2}{3} R_T^3 - R_U R_T^2 + \frac{1}{3} R_U^3 \right) + V_D (r^2 - R_T^2) \right\} \quad (8-9)$$

in the downflow region ($R_T < r < R$).

For a granule of radius 500 km (and thus with $R_U = 340$ km and $R_T = 460$ km), equal to the mean solar granule radius, and the vertical velocity parameters used in this work (see table 8-2 for the parameter values), the horizontal velocities are shown in figure 8-19.

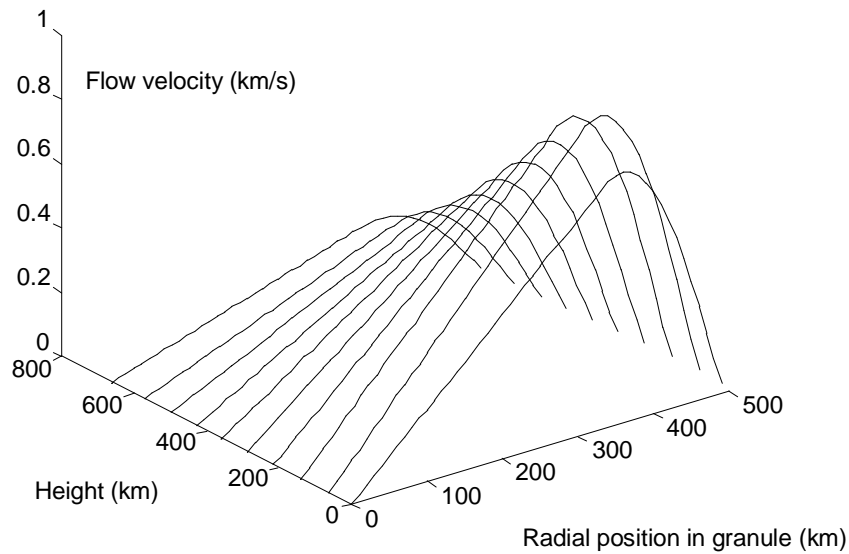


Figure 8-19: Variation of Horizontal Flow

The mean outward flow velocity (weighted by area) and the peak outward flow velocity at different heights in the photosphere are shown in figure 8-20.

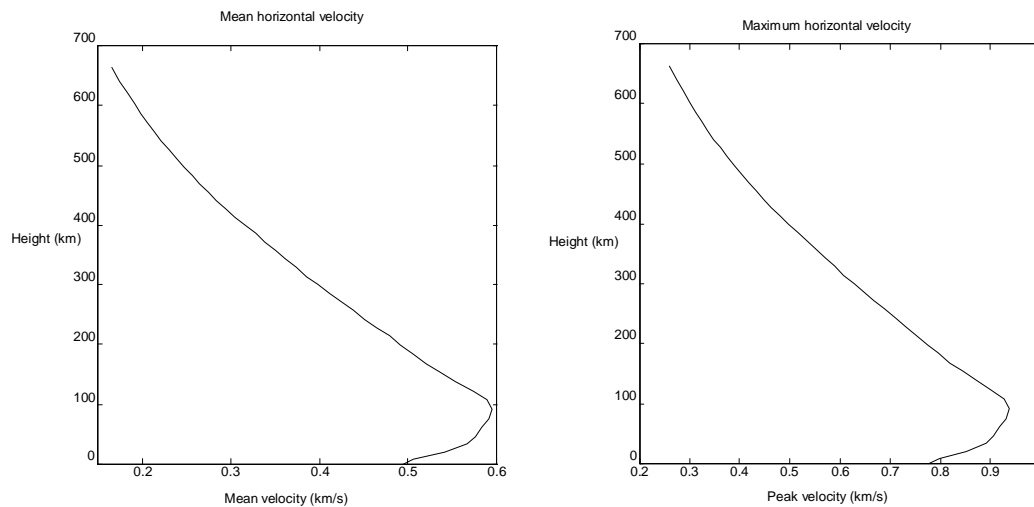


Figure 8-20: Outward Horizontal Flow

From figures 8-19 and 8-20, it can be seen that the horizontal flow velocities decrease with increasing height. The mean outward flow velocity can be compared with the upward flow velocity (see figure 8-21). As the height increases, the horizontal velocity becomes larger compared to the vertical velocity.

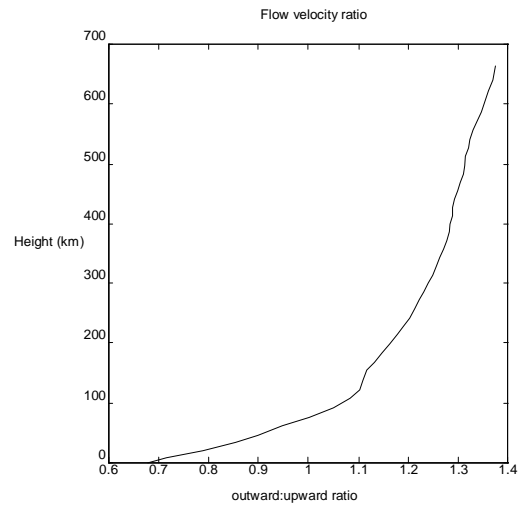


Figure 8-21: Ratio of Outward to Upward Flow Velocities

The overall flow velocities (combining the vertical and horizontal flows) in the photosphere are shown in figure 8-22.

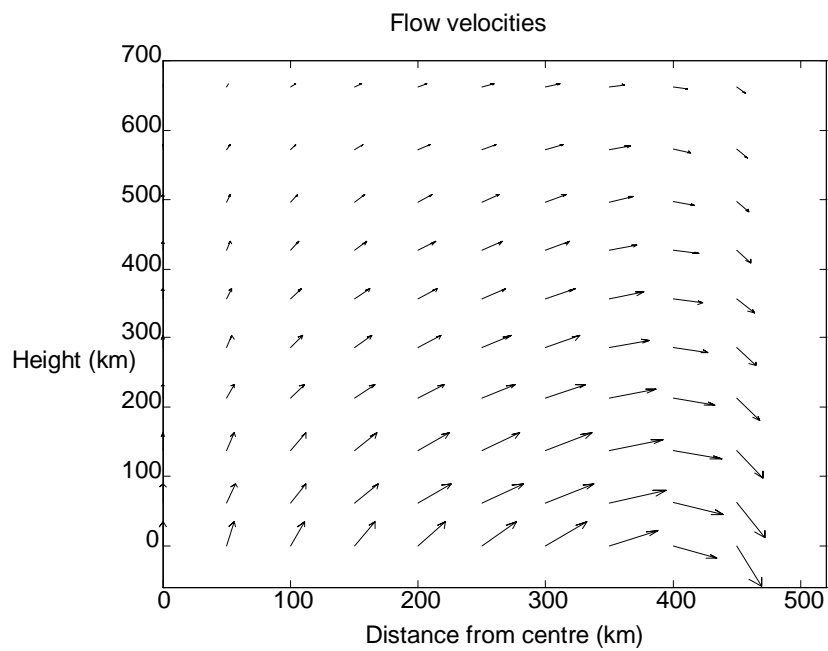


Figure 8-22: Granular Flow within the Photosphere

The distribution of line-of-sight velocities is also of interest. The line-of-sight velocity distribution at the extreme limb at a height of 100 km is shown in figure 8-23.

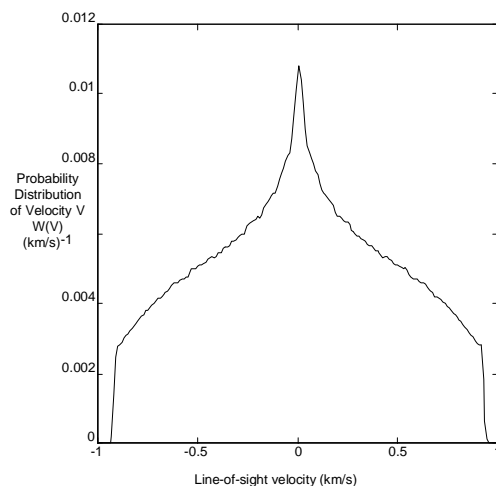


Figure 8-23: Velocity Distribution of Horizontal Flow

The distribution of line-of-sight velocities due to horizontal motions is far from Gaussian. The wings of the distribution are quite strong, and it can be expected that spectral lines observed near the limb will be broadened relative to lines observed closer to disk centre. This distribution is the velocities observed in a single granule; intergranular variations (which are approximately Gaussian) will modify the distribution seen across a larger area of the solar surface.

So far only the horizontal motions associated with circular granules have been considered. If a complete treatment of the problem is desired, it will be necessary to consider the distribution of granule shapes as well.

As the microturbulence is isotropic, the effects of microturbulence will be identical whether horizontal or vertical velocities are being considered.

8.4.3: Spectral Synthesis with Horizontal Motions

With the horizontal motions known, spectra affected by horizontal motions can be calculated. Spectra emergent from positions other than the centre of the solar disk can thus be found. In practice, this involves significant difficulties not encountered in the vertical velocity disk centre case. The simplicity of the granular cell model used in this work was only possible due to the passage of emergent radiation through relatively

uniform regions allowing division of the granular cell into a small number of regions. This will no longer be the case away from disk centre. (See figure 8-24.)

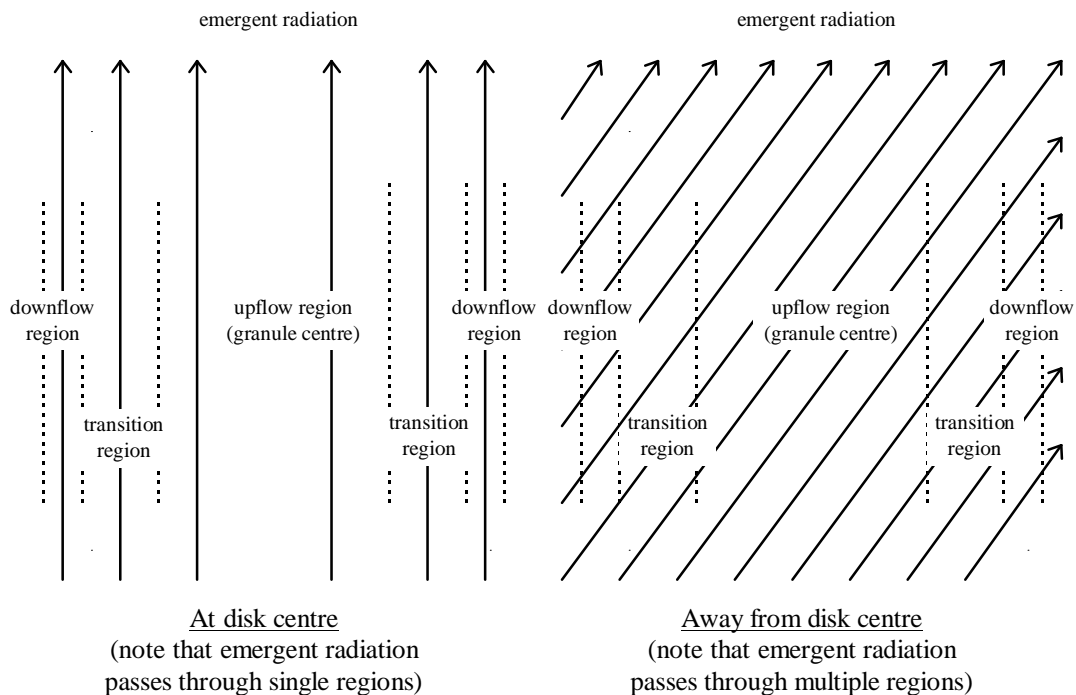


Figure 8-24: Radiation Emergent Away from Disk Centre

With the radiation no longer emergent from single regions, the various combinations of regions through which the radiation passes must be considered. There are a large number of such combinations, particularly if the variations in granule size and geometry are considered. As a result, if a multiple-region plane-parallel method is to be used to calculate the emergent spectrum, a large number of regions must be considered. This is particularly important for strong lines, as the low correlation between the velocities in the regions the radiation passes through will result in an increase in the equivalent width of the line, independently of other increases in the equivalent width.

As the emergent spectrum away from disk centre depends on the size of the granulation, a suitable granule size parameter must be introduced into the model. This is not necessary at disk centre, as the size of the granulation does not directly affect the spectrum. As the size of granules can be directly observed, this should not present too great a difficulty.

Although the calculation of spectra from arbitrary points on the solar disk is a difficult procedure compared to calculation of the disk centre spectrum, for a few cases, suitable approximations allow calculations to be performed.

At positions away from, but close to, disk centre, the emergent spectrum can be calculated using the disk centre model, but with slight modifications to the velocity fields to account for the line-of-sight component of the horizontal mass flow velocity field and the effect of horizontal motions on the macroturbulence parameter.

For very weak lines, the intensity of the emergent radiation is almost constant across the spectral line, and is close to the continuum intensity. As a result of this, the equivalent width of the spectral line is almost independent of the velocity fields. (Unlike strong lines, where the equivalent width depends on both velocity gradients and the microturbulence.) A multi-stream model is not necessary in this case as the velocity distribution can be used to broaden the line profile at any depth without regard to the correlations between flow velocities and microturbulence along the line-of-sight for the emergent radiation.

A simple scheme to calculate emergent spectra away from disk centre that uses elements of both of these approximations is to use the standard three-column model used in this work, with the effective microturbulence at any depth given by combining the actual microturbulence $\xi(\tau)$ and the line-of-sight component of the horizontal flow field, assumed to be Gaussian, with a mean of $V_H(\tau)$, giving

$$\xi_{eff}(\tau) = \sqrt{\xi(\tau)^2 + V_H(\tau)^2(1 - \mu^2)} \quad (8-10)$$

where $\mu = \cos \theta$. The mean horizontal flow speed can be found from the vertical flow speed, using equations (8-7), (8-8) and (8-9). Near the limb, it will no longer be an adequate approximation to use the microturbulence for a particular region, as the emergent radiation will pass through multiple regions. The microturbulence at the extreme limb will effectively be the mean microturbulence

$$\bar{\xi}(\tau) = \sum_{\substack{\text{all} \\ \text{regions}}} A_i B_i \xi_i(\tau). \quad (8-11)$$

The effective microturbulence in a region i can be found by a weighted combination of the mean microturbulence and the region microturbulence, giving an effective microturbulence (considering horizontal motions as well) of

$$\xi_{eff}(\tau) = \sqrt{\xi_i(\tau)^2 \mu^2 + \bar{\xi}(\tau)^2(1 - \mu^2) + V_H(\tau)^2(1 - \mu^2)}. \quad (8-12)$$

Similarly, the macroturbulence can be found from the line-of-sight component of the vertical macroturbulence, and the line-of-sight component of the horizontal macroturbulence, giving

$$\Xi_{eff} = \sqrt{\Xi_v^2 \mu^2 + \Xi_H^2 (1 - \mu^2)}. \quad (8-13)$$

The horizontal macroturbulence can be found from the mean vertical macroturbulence, increased by the outward:upward velocity ratio (see figure 8-21), giving

$$\Xi_H = \sum_{\substack{\text{all} \\ \text{regions}}} A_i B_i \Xi_{v_i} \quad (8-14)$$

where A_i and B_i are the area and brightness parameters for the region i . The results of this procedure are compared to observations of the centre-to-limb variations (CLV) in section 8.6.1.

Related to the problem of calculating spectrum emergent from positions away from disk centre is the calculation of the spectrum averaged over the entire disk. A full treatment requires the calculation of spectra from a number of separate positions on the disk, and, after taking rotation of the sun (or other star) into account, combining these into an average spectrum. This is necessary for a full calculation of the spectrum of a star for comparison with the observed stellar spectrum. In view of the difficulty of such a procedure, the stellar surface is often approximated as a disk centre atmosphere.⁶

⁶This was done by Dravins in Dravins, D. "Stellar Granulation VI: Four-Component Models and Non-Solar-Type Stars" *Astronomy and Astrophysics* **228**, pg 218-230 (1990). This allowed a simple model similar to the disk centre model used in this work to be used.

8.5: The Granular Cell Model and Granulation Simulations

The granular cell model adopted in this work is based directly on observations of the solar granulation. Numerical simulations which reproduce the appearance of the solar granulation can be compared with the model. Unlike the actual solar granulation, simulations permit detailed knowledge of the conditions in the (simulated) photosphere, including velocities not readily observed in the sun.

The difficulty in comparing results of the adopted parametric model with simulation results is that emergent spectra from simulations must be calculated over a sufficiently long time period to give a stable average spectrum. Instantaneous spectra from simulated convection show a wide variety of profiles, including profiles with asymmetry opposite to that usually seen. As longer time periods are taken into account, the average spectrum more closely resemble the solar spectrum.⁷

How closely simulated granulation agrees with the parametric model used in this work is more a question of how closely such simulations agree with the convection observed in the photosphere. As simulations reproduce the solar granulation reasonably well, the agreement between the adopted parametric model and simulations is quite good. As the parametric granular model is independent of granule size (as far as other properties of the granulation are size-independent), the agreement can be even closer than that between simulations and the granulation.⁸

⁷ Dravins, D., Lindegren, L. and Nordlund, Å. "Solar Granulation: Influence of Convection on Spectral Line Asymmetries and Wavelength Shifts" *Astronomy and Astrophysics* **96**, pg 345-364 (1981).

⁸ Gadun, A.S. and Vorob'yov, Yu.Yu. "Artificial Granules in 2-D Solar Models" *Solar Physics* **159**, pg 45-51 (1995) where discrepancies in granule size between simulations and observations are discussed.

8.6: The Granular Cell Model and Observations

As the granular model used in this work was derived from observations of the solar granulation, it reproduces the major characteristics of the granulation. Other observational evidence can be used to evaluate the success of the model.

The major tool for comparison is the solar spectrum. The granular model closely reproduces the asymmetry seen in solar photospheric lines, as seen in section 8.3. At the very least, this shows that the granular cell model is suitable for calculating the profiles of solar spectral lines and fitting observed and computed spectra to determine spectral line parameters. The calculated and observed high-spatial resolution spectra emergent from different regions are also very similar (see section 8.3.3).

It should also be noted that depth dependence of the microturbulence is often found using single-stream microturbulence-macroturbulence models. The microturbulence is usually (but not always⁹) found to decrease with increasing height,¹⁰ as is the case here.

8.6.1: Centre-to-Limb Line Variations

As discussed in section 8.4.3, the spectrum emergent at disk positions away from disk centre can be calculated using the horizontal motions. Fraunhofer lines in the solar spectrum increase in equivalent width and FWHM as the limb is approached. This is expected due to the increased importance of horizontal velocities, which will act to broaden spectral lines rather than shift them, unlike vertical flows.

⁹Kostic found an increase in microturbulence with height in Kostic, R.I. “Damping Constant and Turbulence in the Solar Atmosphere” *Solar Physics* **78**, pg 39-57 (1982).

¹⁰See, as an example, the microturbulence (which decreases with height) in the original Holweger-Müller model atmosphere in Holweger, H. and Müller, E.A. “The Photospheric Barium Spectrum: Solar Abundance and Collision Broadening of Ba II Lines by Hydrogen” *Solar Physics* **39**, pg 19-30 (1974).

The difference in wavelength shifts of spectral lines emergent from disk centre and near the limb is readily reproduced by the adopted granulation model. The horizontal motions are symmetric, and will not result in a wavelength shift. The wavelength shift observed at disk centre is due to the strength of the contribution to the emergent spectrum due to the large, bright, rising granular centre. The wavelength shift of this contribution decreases as the limb is approached as the line-of-sight mean velocity of the region becomes smaller.

As the velocity distribution becomes more symmetric as the limb is approached, the asymmetry of spectral lines should decrease. This is confirmed by observations.¹¹

As discussed in section 8.4.3, the spectrum away from disk centre can be approximately calculated. The results of such calculations can be compared to observations of the centre-to-limb variations of spectral lines. The centre-to-limb variations for the Fe I line at 5930.182\AA was calculated. The disk centre spectrum of the line is shown in figure 8-25.

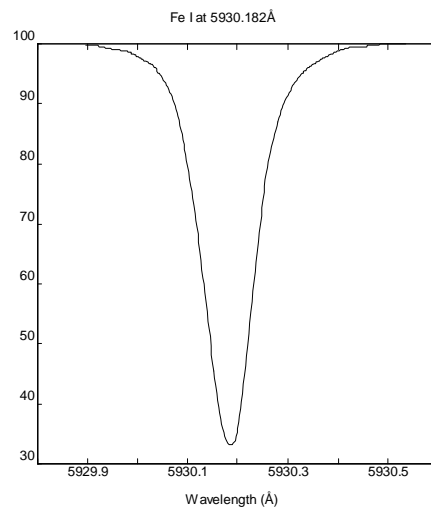


Figure 8-25: Disk Centre Spectrum of Fe I at 5930.182\AA

The calculated and observed centre-to-limb variations of the Fe I line at 5930.182\AA are shown in figures 8-26, 8-27 and 8-28.¹²

¹¹ Marmolino, C., Roberti, G. and Severino, G. "Line Asymmetries and Shifts in the Presence of Granulation and Oscillations: The CLV of the K I 7699 Resonance Line" *Solar Physics* **108**, pg 21-33 (1987).

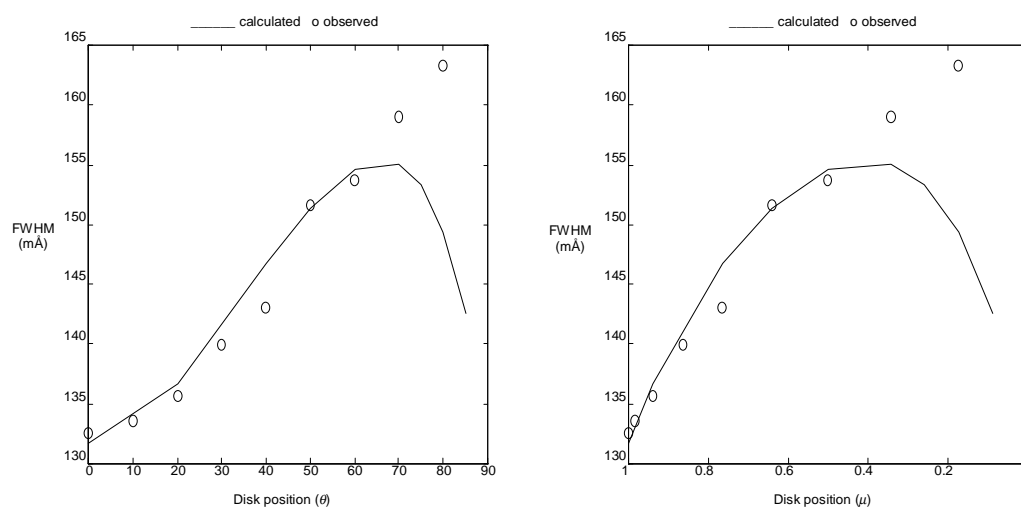


Figure 8-26: FWHM CLV of Fe I at 5930.182\AA

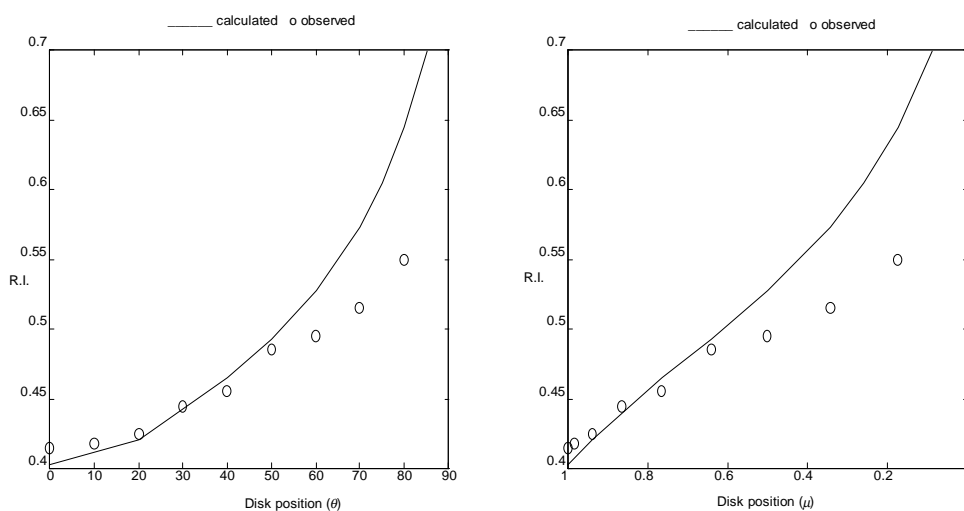


Figure 8-27: Residual Intensity¹³ CLV of Fe I at 5930.182\AA

¹²Observations of the CLV for this line are from Rodríguez Hidalgo, I., Collados, M. and Vázquez, M. “Variations of Properties of the Quiet Photosphere along the Equator and the Central Meridian: Spectroscopic Results” *Astronomy and Astrophysics* **283**, pg 263-274 (1994). The observations have been normalised to match the calculations at disk centre.

¹³The residual intensity is the intensity minimum of the line (i.e. the central intensity). It is given here as a fraction of the continuum.

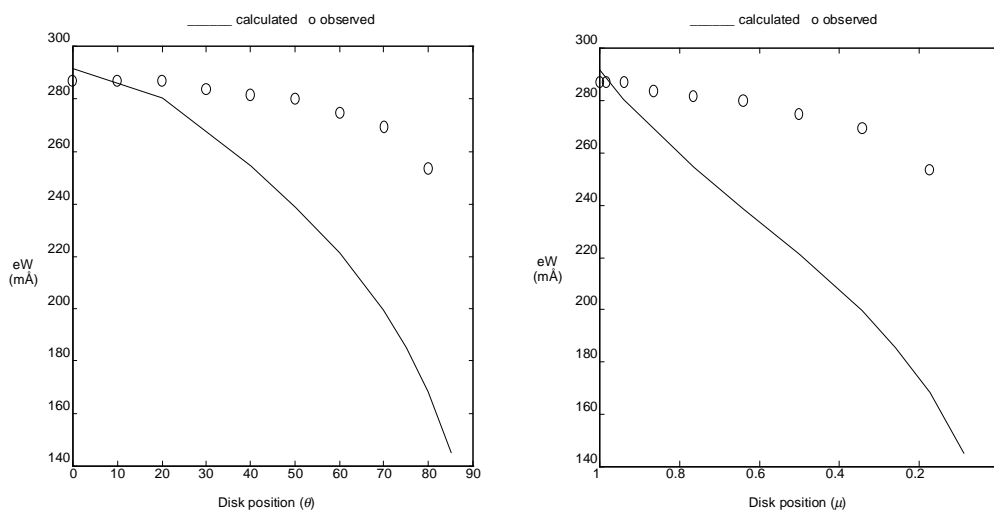


Figure 8-28: Equivalent Width CLV of Fe I at 5930.182Å

The observed and calculated CLV curves for the FWHM and residual intensity agree well near disk centre. The observed and calculated values diverge as the limb is approached, where the approximations employed in the calculation break down. The observed equivalent width falls off much more slowly than the calculated equivalent width. The close agreement between the observed and calculated residual intensity and FWHM lead one to expect a similar agreement between the equivalent widths.

The calculated equivalent widths should be too low near the limb due to the approximations employed. The high velocity gradients through which the emergent radiation must pass, which are not accounted for in the approximate calculations, will result in a strengthening of the line, particularly for a line as strong as the line calculated here.

The centre-to-limb variations of the equivalent widths of a number of lines were measured by Kostic.¹⁴ Calculated centre-to-limb variations are compared to these observations in figure 8-29 and 8-30.

¹⁴Kostic, R.I. "Damping Constant and Turbulence in the Solar Atmosphere" *Solar Physics* **78**, pg 39-57 (1982).

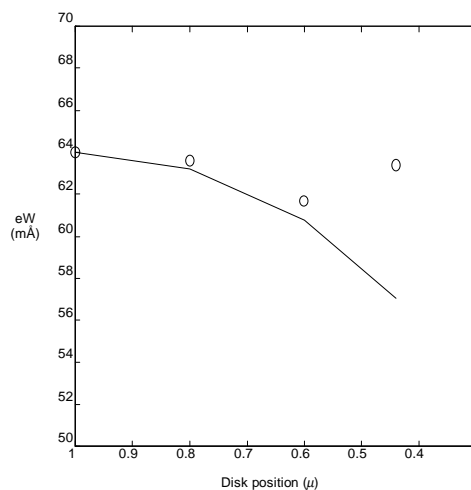


Figure 8-29: Equivalent Width CLV of Ni I at 6176.818Å

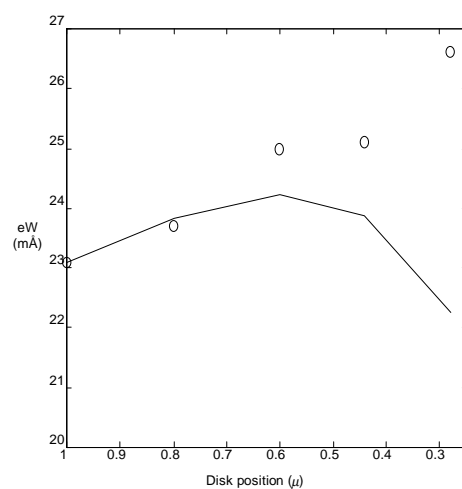


Figure 8-30: Equivalent Width CLV of Fe I at 6786.863Å

The calculated variations reproduce the observations until the limb is approached, when, as expected, the calculated equivalent width becomes too low.

The appearance of a spectral line observed in the flux spectrum (i.e. the spectrum averaged over the entire solar disk) is also of interest. For stars other than the sun, this is all that can be observed as the disk cannot be resolved. The flux spectrum can be calculated by combining centre-to-limb spectra calculated at various disk positions, taking limb darkening and Doppler shifts due to solar rotation into

account. A calculated flux spectral line is shown in figure 8-31 compared with the observed flux line.¹⁵

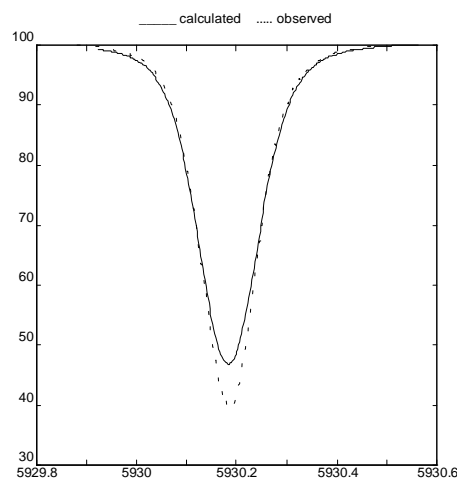


Figure 8-31: Flux Spectrum of Fe I at 5930.182Å

The overall shape of the observed flux spectral line is predicted by the calculated spectral line. The wings of the observed line, and the asymmetry of the line are closely matched by the calculated spectrum. The depth of the line core is poorly matched, as the calculations underestimate the depth of the spectral line.

The calculations of centre-to-limb variations show that the horizontal motions determined from the vertical flow in the granular cell model accurately predict the variation of spectral lines away from, but within a reasonable distance of, disk centre. This lends strong support to the reliability of the parametric granular model. The success of the approximate calculations performed here points to the likelihood of obtaining accurate results if the difficult accurate calculations are performed. As flux spectral line shapes can be predicted, a granular model similar to the one used here can be used in cases where only the flux spectrum is available, such as for other stars.

¹⁵The NSO/Kitt Peak data used here were produced by NSF/NOAO.

8.6.2: Sunspots

Differences between spectra emergent from sunspots and the quiet photosphere should be explainable in terms of the differences in convective flow between the two regions. Spectral lines emergent from sunspots are less broadened than normal spectral lines, indicating lower convective velocities. With high resolution sunspot spectra and an atmospheric model for sunspots, it is possible to investigate convective motions in sunspots using a similar parametric model. With lower convective velocities, and smaller associated line shifts and asymmetry than in the quiet photosphere, the required spectral resolution would be quite high.

8.7: Stellar Spectra

Convective motions in stars other than the sun cannot be directly observed, but can be investigated by examining the asymmetries present in stellar spectral lines. As would be expected, stars similar to the sun exhibit similar line asymmetries,¹⁶ indicating the presence of convective motions similar to those in the sun. A granular cell model very similar to the one used in this work could be used for these stars.

Other (non-solar type) stars show quite different asymmetries in lines in their spectra. Sirius (spectral type A1 V), for example, has a spectrum in which spectral lines are very broad (due to the higher temperatures and high rotation speed) and relatively symmetric. In this case, due to the broadness of the lines, it would be difficult to determine convective motions to any real degree of accuracy. Canopus (F0 II), on the other hand, has spectral lines showing asymmetry opposite to that seen in solar lines, with a strengthened blue wing. This effect is clearly visible, and indicates the presence of rapid upward motions occupying a small area of the stellar surface. Thus, in at least some stars, photospheric motions are quite different to those observed in the solar photosphere. These motions can be investigated using models similar to

¹⁶Dravins, D. "Stellar Granulation II. Stellar Photospheric Line Asymmetries" *Astronomy and Astrophysics* **172**, pg 211-224 (1987).

the solar granular cell model used here, but the results will be uncertain, as there is no guarantee that the model adequately describes the motions actually present.